

Field-sweep-rate and time dependence of transverse resistivity anomalies in ultrathin SrRuO₃ films

Daisuke Kan ^{1,*}, Takahiro Moriyama ^{1,†} and Yuichi Shimakawa ^{1,2}

¹*Institute for Chemical Research, Kyoto University, Uji, Kyoto 611-0011, Japan*

²*Integrated Research Consortium on Chemical Sciences, Uji, Kyoto 611-0011, Japan*



(Received 22 September 2019; revised manuscript received 8 January 2020; published 30 January 2020)

We investigated the field-sweep-rate and time dependence of the transverse resistivity anomalies in ultrathin SrRuO₃ epitaxial thin films the behaviors of which resemble what has been claimed to be the topological Hall effect. We find that the magnitudes of the anomalies are independent of the field sweep rate, while the magnetic field at which the anomalies appear (H_{hump}) and the coercive field (H_c) exhibit identical sweep-rate dependence. We also show that the transverse resistivity under a fixed external magnetic field exhibits transient behavior, eventually (≈ 5000 s) approximating the value of the anomalous Hall resistivity that is obtained after the magnetization reversal processes are completed. These results indicate that H_c is inhomogeneous within the films and activation energies of the magnetization reversal at H_{hump} and H_c are identical. The observed field-sweep-rate and time dependence of the transverse resistivity anomalies can be understood in the framework of conventional magnetic switching dynamics, and topological interpretation would not be necessarily taken into account. Our results are in line with a model in which inhomogeneity of H_c and anomalous Hall resistivity are responsible for the transverse resistivity anomalies in SrRuO₃.

DOI: [10.1103/PhysRevB.101.014448](https://doi.org/10.1103/PhysRevB.101.014448)

I. INTRODUCTION

When conduction electrons in magnetic materials and artificial heterostructures are coupled with magnetization, a Berry-curvature-originated fictitious magnetic field plays a key role in transport behavior and is manifested as additional transverse electron scattering, leading to various types of the Hall effect, such as the anomalous Hall effect (AHE) in ferromagnets [1–4] and antiferromagnets [5,6] and the topological Hall effect (THE) [7–9]. Because Berry curvatures are often correlated to (topologically) nontrivial electronic structures and magnetic spin textures, exploring such Hall effects has attracted attention and has been one of the hot topics in condensed matter physics. In fact, recent reports have showed that various magnetic materials and artificial heterostructures including heterostructured oxides display anomalies in the transverse resistivity and have discussed their possible attribution to the THE due to the formation of skyrmions [10–19].

The ferromagnetic perovskite oxide SrRuO₃ (SRO) having large uniaxial magnetic anisotropy exhibits unique magnetotransport properties such as temperature-induced sign reversal of the AHE, in which Berry curvature arising from multiple band crossings around the Fermi level E_F is manifested [20–22]. Recently, ultrathin films of SRO have been reported to exhibit anomalies in transverse resistivity that are associated with field-induced magnetic reversal. While the anomalies cannot be explained by the conventional framework of AHE and are often attributed to the emergence of the THE [11,23–25], their origin has still been under debate and alternatives to the topological interpretation have been

proposed [26–28]. Inhomogeneity in the coercive field (H_c) and the anomalous Hall coefficient (ξ), which are possibly originated from nonuniform thickness and/or Ru deficiencies [26,29], have been shown to lead to hump structures (referred to as hump resistivity ρ_{hump}) in the field dependence of the anomalous Hall resistivity (ρ_{AHE}) and to be the possible origin of the transverse resistivity anomalies [Fig. 1(a)] [27].

Magnetization reversal processes in magnetic materials are of a first-order nature and thus strongly depend on either sweep rates of external magnetic fields or periods of measuring time [30–32]. In the framework of conventional ferromagnetic domain nucleation and expansion, the coercive field H_c (or the switching field) varies depending on the sweep rate of the magnetic field R_H and is known to take the following form:

$$\langle H_c \rangle = H_{c0}(T) \left\{ 1 - \left[\frac{k_B T}{E_a} \ln \left(\frac{1}{\tau_0 |R_H| \ln 2} \right) \right]^{2/3} \right\} \quad (1)$$

where $H_{c0}(T)$ is the coercive field in absence of thermal fluctuation, k_B is the Boltzmann constant, T is the temperature, E_a is the activation energy, and τ_0 is the inverse of the attempt frequency which is assumed to be 10^{-9} s. This R_H dependence of H_c leads to changes in the magnetic field dependence of the magnetization and the anomalous Hall resistivity (ρ_{AHE}), as shown in Fig. 1(b). When ferromagnetic domains having positive and negative ξ coexist (like SRO films), not only H_c but also the hump field H_{hump} , which is defined as the field at which the ρ_{hump} is seen in the $\rho_{\text{AHE}}-H$ curve, should be R_H dependent following Eq. (1). On the other hand, the ρ_{hump} should be R_H independent unless the ρ_{hump} is attributed to formations of nontrivial magnetic spin textures such as skyrmions. Given that the magnitude of THE is proportional to the density of skyrmions formed by the field sweeps, the

*dkan@scl.kyoto-u.ac.jp

†mtaka@scl.kyoto-u.ac.jp

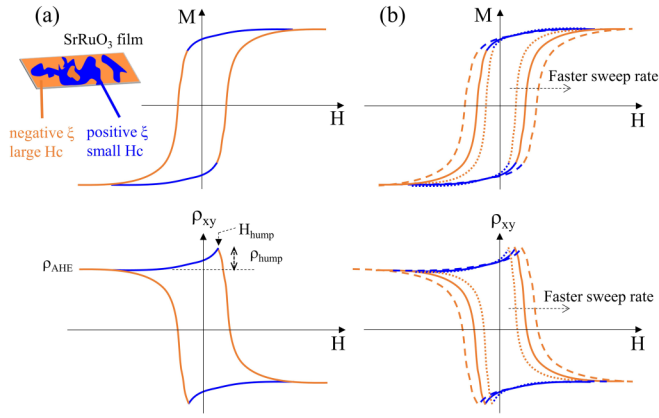


FIG. 1. (a) Schematic drawing of the magnetic field dependence of the magnetization M and the anomalous Hall resistivity ρ_{AHE} for SrRuO₃ films in which the coercive field (H_c) and ρ_{AHE} are inhomogeneous. The regions colored with orange in the film have large H_c and negative anomalous Hall coefficient (ξ) while the region colored blue has small H_c and positive ξ . (b) Expected variations of M - T and ρ_{AHE} - T curves obtained at different field sweep rates.

topological interpretation suggests R_H -dependent changes in the ρ_{hump} . In this paper, we investigate the field-sweep-rate R_H and time dependence of the transverse resistivity anomalies in ultrathin SRO epitaxial films the behavior of which resembles what has been claimed to be the topological Hall effect [11,23–25]. We found that both the field sweep rate and the period of the measuring time influence behaviors of the anomalies (or ρ_{hump}) in ultrathin SRO films. We analyze the R_H - and time-dependent behaviors of the anomalies and discuss their origin.

II. EXPERIMENTAL DETAILS

SRO thin films (3.5 nm thick) were deposited on (110) NdGaO₃ substrate by pulsed laser deposition. Details of the film growth were given in our previous reports [33,34]. X-ray-diffraction measurements confirmed that the SRO films were epitaxially and coherently grown on the substrate. For transport measurements, a 50- μm -wide Hall bar was fabricated by conventional photolithography and Ar ion milling. We confirmed from the temperature dependence of the electrical resistivity that the film exhibits metallic conduction down to low temperatures and undergoes ferromagnetic transition at 115 K.

III. RESULTS AND DISCUSSION

Figure 2(a) shows the magnetic field dependence of the anomalous part of transverse resistivity (the anomalous Hall resistivity ρ_{AHE}) for the 3.5-nm-thick SRO film measured at various temperatures. Transverse resistivity was measured by a standard lock-in technique with an excitation current of 30 μA sinusoidally alternating at 13 Hz. The magnetic field was swept at a rate of 10 Oe/s. To obtain ρ_{AHE} , the measured transverse resistivity was antisymmetrized and the ordinary part of the transverse resistivity was subtracted. The ρ_{AHE} at high temperatures (for example, at 68 K) is positive. With decreasing temperature, it decreases and undergoes

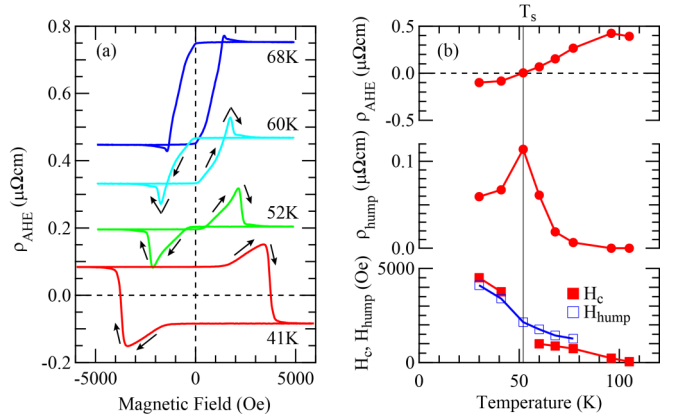


FIG. 2. (a) Magnetic field dependence of the anomalous Hall resistivity ρ_{AHE} for the 3.5-nm-thick SrRuO₃ film measured at various temperatures. Every loop in the figure has an offset of 0.2 $\mu\Omega\text{cm}$. (b) Anomalous Hall resistivity ρ_{AHE} , hump resistivity ρ_{hump} , coercive field H_c , and hump field H_{hump} plotted as functions of temperature. The definitions of ρ_{hump} and H_{hump} are provided in Fig. 1. We note that, at T_s , ρ_{AHE} becomes almost zero, which makes it difficult to determine H_c in the ρ_{AHE} - H curve.

sign reversal at 52 K. Hereafter this unique temperature at which ρ_{AHE} becomes zero is denoted T_s . The temperature-dependent changes in ρ_{AHE} are in close agreement with those in the previous reports and are ascribed to the temperature-induced changes in the integrated Berry curvature over conduction bands [21]. In addition, in the ρ_{AHE} - H loops at low temperatures, humps associated with the field-induced magnetization reversal are seen. We defined the hump resistivity ρ_{hump} as the height of the loops and the hump field H_{hump} as the field at which the hump is located [see Fig. 1(a)]. In Fig. 1(b) (and Fig. S1 in the Supplemental Material [35]) we plot ρ_{hump} and H_{hump} as a function of temperature, together with ρ_{AHE} and the coercive field H_c . It is seen that, as the temperature approaches T_s , ρ_{AHE} , ρ_{hump} , and H_c concomitantly change. When ρ_{AHE} is zero at T_s , the ρ_{hump} is maximized. H_c and H_{hump} increase with decreasing temperature. It should be noted that ρ_{AHE} at T_s is almost zero and extracting H_c is difficult. Although it has been discussed that ρ_{hump} is a hallmark of the emergence of the topological Hall effect and that ρ_{hump} should behave independent of ρ_{AHE} [11,23], the observed behaviors of the transverse resistivity in Fig. 1(b) imply that ρ_{hump} is correlated with ρ_{AHE} and the origins of these two resistivities are the same [26], supporting the model in which ρ_{AHE} and H_c in the ultrathin SRO films are not spatially homogeneous and that magnetization-reversal-induced variations in distributions of positive and negative ρ_{AHE} lead to the emergence of ρ_{hump} [27].

We now look into the field-sweep-rate (R_H) dependence of transverse resistivity in the SRO film. The results are summarized in Fig. 3. The ρ_{AHE} - H curves with the R_H of 2, 5, 10, and 20 Oe/s were measured at 41, 50, and 60 K. The curves in Figs. 3(a), 3(c), and 3(e) were obtained by first applying a negative magnetic field (−6000 Oe) much larger than H_c and sweeping the field toward the positive-field region. Regardless of the measuring temperature, both H_{hump} and H_c are found to become larger with increasing the R_H ,

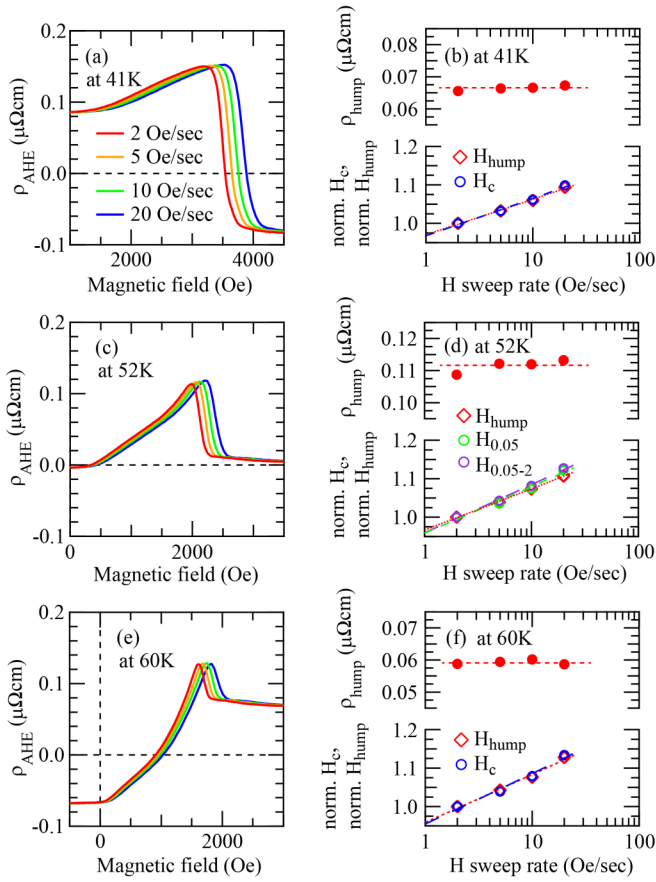


FIG. 3. (a, c, e) Magnetic field dependence of the transverse resistivity measured with various field sweep rates R_H at (a) 41 K, (c) 52 K, and (e) 60 K. (b, d, f) R_H dependence of the hump resistivity ρ_{hump} , hump field H_{hump} , and coercive field H_c at (b) 41 K, (d) 52 K, and (f) 60 K. In the bottom panels of (b), (d), and (f), the H_{hump} and H_c are normalized by those obtained with the sweep rate of 2 Oe/s and the dotted line shows the best fits to Eq. (1). The fitting parameters are summarized in Table I. Note that at 52 K, where ρ_{AHE} is almost zero, H_c is difficult to extract from the $\rho_{\text{AHE}}-H$ curves and therefore the magnetic fields at which ρ_{AHE} becomes $0.05 \mu\Omega \text{ cm}$ (referred to as $H_{0.05}$ and $H_{0.05-2}$), are used for the fitting.

while the transverse resistivity at H_{hump} (ρ_{hump}) is almost R_H independent. These observations are in agreement with the expected behavior in Fig. 1. Figures 3(b), 3(d), and 3(f) show the R_H dependence of ρ_{hump} , H_{hump} , and H_c at each measuring temperature. In each plot, both H_{hump} and H_c are normalized by those obtained with the sweep rate of 2 Oe/s. In addition to the observation of the R_H independence of the transverse resistivity at H_{hump} (namely, ρ_{hump}), the R_H dependences of the normalized H_{hump} and H_c at each temperature are found to fall into the single trend. We fit the R_H dependences of H_{hump} and H_c [Figs. 3(b), 3(d), and 3(f)] with Eq. (1) and evaluated $H_{c0}(T)$ and E_a . The values obtained are summarized in Table I. Regardless of the measuring temperatures, the E_a determined from the H_c and the E_a determined from the H_{hump} are about the same, implying that the mechanisms behind magnetization reversal processes at H_{hump} and H_c are identical and governed by conventional ferromagnetic domain nucleation and expansion. These field-sweep-rate dependences of

TABLE I. The activation energy E_a and the coercive field in absence of thermal fluctuation $H_{c0}(T)$ evaluated by fitting the field-sweep-rate dependence of the coercive field H_c and the hump field H_{hump} with Eq. (1). Note that at 52 K, where ρ_{AHE} is almost zero, H_c is difficult to extract from the $\rho_{\text{AHE}}-H$ curves. Therefore, the magnetic fields at which ρ_{AHE} becomes $0.05 \mu\Omega \text{ cm}$ (referred to as $H_{0.05}$ and $H_{0.05-2}$) are analyzed.

Temperature		E_a (eV)	H_{c0} (Oe)
41 K	H_{hump}	0.18 ± 0.01	7072 ± 189
	H_c	0.17 ± 0.01	8055 ± 292
52 K	H_{hump}	0.20 ± 0.01	4770 ± 60
	$H_{0.05}$	0.19 ± 0.01	3213 ± 165
	$H_{0.05-2}$	0.19 ± 0.01	5685 ± 182
60 K	H_{hump}	0.21 ± 0.01	4254 ± 206
	H_c	0.21 ± 0.01	2466 ± 148

the transverse resistivity anomalies can be understood in the framework of conventional magnetic switching dynamics, and topological interpretation would not be necessarily taken into account. However, how formations of topological magnetic structures affect magnetic switching dynamics has not been so clear and our results cannot completely exclude possible formations of topological objects such as skyrmionlike magnetic bubbles [17,24,36], which are associated with the magnetization switching. On the other hand, it would not be unreasonable to expect that formations and dynamics of such topological objects and their inducing transverse scatterings of electrons (or topological Hall effect) should depend on the field sweep rate, which is not consistent with our observation of the R_H independence of ρ_{hump} . For further understanding how the field sweep rates affect topological objects' formations and dynamics in oxide heterostructures, their direct observations will be necessary.

We also investigate the time dependence of ρ_{hump} . Figure 4(a) shows the transient behavior of the transverse resistivity

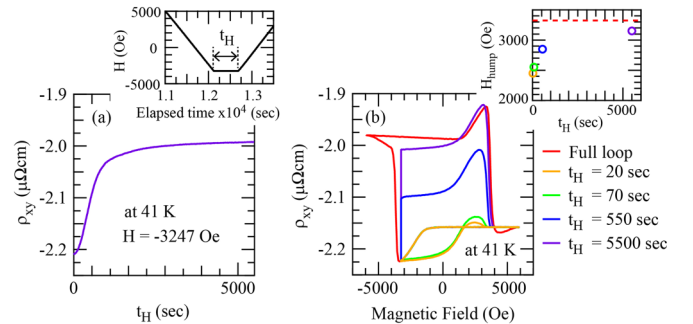


FIG. 4. (a) Time dependence of the transverse resistivity under the fixed magnetic field of -3247 Oe, which corresponds to the negative H_{hump} and at which ρ_{hump} is seen. The data were obtained at 41 K. The inset shows the diagram of the field sweeps and the definition of the time period t_H used for measuring the time dependence of ρ_{hump} . (b) Magnetic field dependence of the transverse resistivity obtained from the time dependent measurements with various t_H . The inset shows the t_H dependence of the positive H_{hump} , which is extracted from the field dependence of the resistivity in (b).

of the SRO films under the negative H_{hump} (-3247 Oe) and at 41 K. Prior to the time-dependence measurements, a positive magnetic field (6000 Oe), which is large enough to saturate the magnetization in the film, was applied and the field was swept toward H_{hump} . When the field reached the negative H_{hump} , the field was fixed for a given duration (t_H) and then swept back from the H_{hump} to the initial positive field. The field sweep diagram for the time-dependence measurement is provided in the inset of Fig. 4(a), and the transverse resistivity ρ_{xy} during the time-dependence measurement is plotted against the magnetic field in Fig. 4(b). The ρ_{xy} plotted were not antisymmetrized. We see in Fig. 4(a) that the transverse resistivity under the fixed negative H_{hump} gradually decreases in its magnitude over time and eventually gets close to the value of ρ_{AHE} . The observed transient behavior implies that under the fixed H_{hump} the magnetization in the film reverses gradually rather than suddenly. Furthermore, the magnetic field dependence of the transverse resistivity in the return sweep in Fig 4(b) strongly depends on the t_H . For the cases with the relatively shorter t_H ($t_H = 20$ and 70 s), the transverse resistivity at the negative H_{hump} remains almost unchanged in the negative-field region of the return sweep. With further sweeping the field back toward the positive magnetic field, it begins to increase and a hump appears at the positive H_{hump} . For the cases with the longer t_H ($t_H = 550$ and 5500 s), the sign of the ρ_{AHE} reverses to the positive in t_H under the fixed negative H_{hump} . While the behavior of the transverse resistivity in the return sweeps is essentially the same as that seen for the shorter t_H case, the ρ_{hump} in the positive field becomes larger with t_H as shown in the inset of Fig. 4(b). These observations indicate that the coercive field in the film is not homogeneous and that consequently even under the fixed external field the magnetization gradually reverses. This inhomogeneity can also explain the t_H -dependent changes in the H_{hump} in the inset of Fig. 4(b). The observed transient behavior of the transverse resistivity is in line with the model described in Fig. 1, indicating that the gradual occurrence of the magnetization reversal due to the inhomogeneous H_c changes the populations of the domains having the positive and negative ρ_{AHE} and consequently leads to the emergence of the ρ_{hump} .

Although the sign of ρ_{AHE} in SRO and the shape of the $\rho_{\text{AHE}}-H$ hysteresis loops are temperature dependent (Fig. 2), the overall trend of the transient behavior of the transverse resistivity remains unchanged. Figure 5 summarizes the transient behavior at 52 K ($=T_s$) and 60 K where the saturated ρ_{AHE} is almost zero and positive. Regardless of the measuring temperature (or the ρ_{AHE} 's value), the transverse resistivity under the fixed H_{hump} (-2053 Oe for 52 K and -1650 Oe for 60 K) gradually increases and gets close to the value of ρ_{AHE} . In the return sweeps from the negative H_{hump} , humps appear in the positive-field region [Figs. 5(b) and 5(d)] and their H_{hump} depends on t_H as shown in the insets of Fig. 5(d). These observed transient behaviors are consistent with the fact that the coercive field in the film is inhomogeneous and the fixed external field leads to gradual occurrence of the magnetization reversal, which is in line with the model in which ρ_{hump} originates from the inhomogeneous distribution of ρ_{AHE} and H_c within the film.

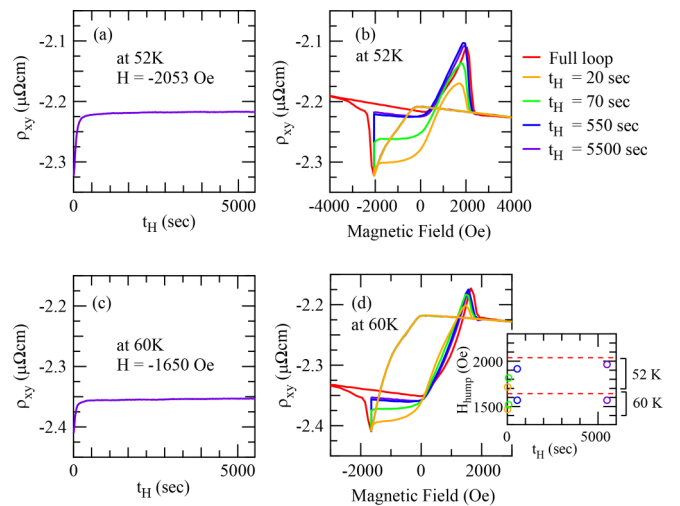


FIG. 5. (a) Time dependence of the transverse resistivity under the negative H_{hump} at 52 K. (b) Magnetic field dependence of the transverse resistivity at 52 K, including the data plotted in (a). (c) Time dependence of the transverse resistivity under the negative H_{hump} at 60 K. (d) Magnetic field dependence of the transverse resistivity at 60 K, including the data plotted in (c). The inset shows the t_H dependence of the positive H_{hump} at 52 and 60 K.

IV. SUMMARY

We investigate the field-sweep-rate and time dependence of the transverse resistivity anomalies in ultrathin SRO epitaxial films. The magnitudes of the anomalies are found to be independent of the field sweep rate, while the field at which the anomalies appear (H_{hump}) exhibits field-sweep-rate dependence the behavior of which is identical to that of the coercive field H_c . The activation energies for the magnetization reversals at H_{hump} and H_c are identical. We also show that the transverse resistivity in the SRO films exhibits transient behavior, revealing that the coercive field is inhomogeneous and that the field-induced magnetic reversal occurs gradually rather than suddenly. These field-sweep-rate and time dependences of the transverse resistivity anomalies can be understood in the framework of conventional magnetic switching dynamics, and topological interpretation would not be necessarily taken into account. The gradual occurrence of the magnetization reversal modifies populations of the magnetic domains having positive and negative ρ_{AHE} , and consequently leads to the emergence of the transverse resistivity anomalies. This is in line with the model in which inhomogeneity in H_c and AHE is the key factor responsible for the transverse resistivity anomalies in SRO films.

ACKNOWLEDGMENTS

This work was partially supported by a grant for the Integrated Research Consortium on Chemical Sciences, by Grants-in-Aid for Scientific Research (Grants No. JP16H02266, No. JP17H05217, and No. JP17H04813), by a Japan Society for the Promotion of Science Core-to-Core program (A), and by a grant for the Joint Project of Chemical Synthesis Core Research Institutions from the Ministry of Education, Culture, Sports, Science, and Technology of Japan.

- [1] N. Nagaosa, J. Sinova, S. Onoda, A. H. MacDonald, and N. P. Ong, *Rev. Mod. Phys.* **82**, 1539 (2010).
- [2] T. Jungwirth, Q. Niu, and A. H. MacDonald, *Phys. Rev. Lett.* **88**, 207208 (2002).
- [3] Y. Yao, L. Kleinman, A. H. MacDonald, J. Sinova, T. Jungwirth, D.-s. Wang, E. Wang, and Q. Niu, *Phys. Rev. Lett.* **92**, 037204 (2004).
- [4] Y. Taguchi, Y. Oohara, H. Yoshizawa, N. Nagaosa, and Y. Tokura, *Science* **291**, 2573 (2001).
- [5] S. Nakatsuji, N. Kiyohara, and T. Higo, *Nature (London)* **527**, 212 (2015).
- [6] T. Suzuki, R. Chisnell, A. Devarakonda, Y. T. Liu, W. Feng, D. Xiao, J. W. Lynn, and J. G. Checkelsky, *Nat. Phys.* **12**, 1119 (2016).
- [7] S. Mühlbauer, B. Binz, F. Jonietz, C. Pfleiderer, A. Rosch, A. Neubauer, R. Georgii, and P. Böni, *Science* **323**, 915 (2009).
- [8] P. Bruno, V. K. Dugaev, and M. Taillefumier, *Phys. Rev. Lett.* **93**, 096806 (2004).
- [9] N. Nagaosa and Y. Tokura, *Nat. Nano.* **8**, 899 (2013).
- [10] M. Uchida and M. Kawasaki, *J. Phys. D* **51**, 143001 (2018).
- [11] J. Matsuno, N. Ogawa, K. Yasuda, F. Kagawa, W. Koshibae, N. Nagaosa, Y. Tokura, and M. Kawasaki, *Sci. Adv.* **2**, e1600304 (2016).
- [12] I. Lindfors-Vrejoiu and M. Ziese, *Phys. Status Solidi B* **254**, 1600556 (2017).
- [13] Y. Ohuchi, Y. Kozuka, M. Uchida, K. Ueno, A. Tsukazaki, and M. Kawasaki, *Phys. Rev. B* **91**, 245115 (2015).
- [14] B. M. Ludbrook, G. Dubuis, A. H. Puichaud, B. J. Ruck, and S. Granville, *Sci. Rep.* **7**, 13620 (2017).
- [15] A. Soumyanarayanan, M. Raju, A. L. Gonzalez Oyarce, A. K. C. Tan, M.-Y. Im, A. P. Petrovic, P. Ho, K. H. Khoo, M. Tran, C. K. Gan, F. Ernult, and C. Panagopoulos, *Nat. Mater.* **16**, 898 (2017).
- [16] S. Woo, K. Litzius, B. Kruger, M.-Y. Im, L. Caretta, K. Richter, M. Mann, A. Krone, R. M. Reeve, M. Weigand, P. Agrawal, I. Lemesch, M.-A. Mawass, P. Fischer, M. Klaui, and G. S. D. Beach, *Nat. Mater.* **15**, 501 (2016).
- [17] L. Vistoli, W. Wang, A. Sander, Q. Zhu, B. Casals, R. Cichelero, A. Barthélémy, S. Fusil, G. Herranz, S. Valencia, R. Abrudan, E. Weschke, K. Nakazawa, H. Kohno, J. Santamaria, W. Wu, V. Garcia, and M. Bibes, *Nat. Phys.* **15**, 67 (2019).
- [18] W. Jiang, X. Zhang, G. Yu, W. Zhang, X. Wang, M. Benjamin Jungfleisch, J. E. Pearson, X. Cheng, O. Heinonen, K. L. Wang, Y. Zhou, A. Hoffmann, and S. G. E. te Velthuis, *Nat. Phys.* **13**, 162 (2017).
- [19] K. Yasuda, R. Wakatsuki, T. Morimoto, R. Yoshimi, A. Tsukazaki, K. S. Takahashi, M. Ezawa, M. Kawasaki, N. Nagaosa, and Y. Tokura, *Nat. Phys.* **12**, 555 (2016).
- [20] G. Koster, L. Klein, W. Siemons, G. Rijnders, J. S. Dodge, C.-B. Eom, D. H. A. Blank, and M. R. Beasley, *Rev. Mod. Phys.* **84**, 253 (2012).
- [21] Z. Fang, N. Nagaosa, K. S. Takahashi, A. Asamitsu, R. Mathieu, T. Ogasawara, H. Yamada, M. Kawasaki, Y. Tokura, and K. Terakura, *Science* **302**, 92 (2003).
- [22] S. Itoh, Y. Endoh, T. Yokoo, S. Ibuka, J.-G. Park, Y. Kaneko, K. S. Takahashi, Y. Tokura, and N. Nagaosa, *Nat. Commun.* **7**, 11788 (2016).
- [23] L. Wang, Q. Feng, Y. Kim, R. Kim, K. H. Lee, S. D. Pollard, Y. J. Shin, H. Zhou, W. Peng, D. Lee, W. Meng, H. Yang, J. H. Han, M. Kim, Q. Lu, and T. W. Noh, *Nat. Mater.* **17**, 1087 (2018).
- [24] K.-Y. Meng, A. S. Ahmed, M. Baćani, A.-O. Mandru, X. Zhao, N. Bagués, B. D. Esser, J. Flores, D. W. McComb, H. J. Hug, and F. Yang, *Nano Lett.* **19**, 3169 (2019).
- [25] Q. Qin, L. Liu, W. Lin, X. Shu, Q. Xie, Z. Lim, C. Li, S. He, G. M. Chow, and J. Chen, *Adv. Mater.* **31**, 1807008 (2018).
- [26] D. Kan and Y. Shimakawa, *Phys. Status Solidi B* **255**, 1800175 (2018).
- [27] D. Kan, T. Moriyama, K. Kobayashi, and Y. Shimakawa, *Phys. Rev. B* **98**, 180408(R) (2018).
- [28] A. Gerber, *Phys. Rev. B* **98**, 214440 (2018).
- [29] L. Wu and Y. Zhang, *arXiv:1812.09847*.
- [30] P. J. Flanders and M. P. Sharrock, *J. Appl. Phys.* **62**, 2918 (1987).
- [31] P. Qingzhi and H. J. Richter, *IEEE Trans. Magn.* **40**, 2446 (2004).
- [32] M. Sharrock and J. McKinney, *IEEE Trans. Magn.* **17**, 3020 (1981).
- [33] D. Kan, M. Anada, Y. Wakabayashi, H. Tajiri, and Y. Shimakawa, *J. Appl. Phys.* **123**, 235303 (2018).
- [34] D. Kan, R. Aso, H. Kurata, and Y. Shimakawa, *J. Appl. Phys.* **113**, 173912 (2013).
- [35] See Supplemental Material at <http://link.aps.org/supplemental/10.1103/PhysRevB.101.014448> for the magnetic field dependence of ρ_{xx} and ρ_{AHE} , and the temperature dependence of ρ_{xx} , ρ_{AHE} , and H_c .
- [36] X. Yu, Y. Tokunaga, Y. Taguchi, and Y. Tokura, *Adv. Mater.* **29**, 1603958 (2017).